AIAA 2003-0451

The Application of a Wall Interference Correction Method to Flat Plate Models

N. Ulbrich
Sverdrup Technology, Inc.
Moffett Field, California 94035-1000

K. R. Cooper
Institute for Aerospace Research, NRC
Ottawa, Canada

41st AIAA Aerospace Sciences Meeting & Exhibit
6-9 January 2003 / Reno, Nevada

AIAA–2003–0451

THE APPLICATION OF A WALL INTERFERENCE CORRECTION METHOD TO FLAT PLATE MODELS

N. Ulbrich*
SVERDRUP Technology, Inc.
NASA Ames Research Center, Moffett Field, California 94035–1000

K. R. Cooper**
Institute for Aerospace Research
National Research Council, Ottawa, Ontario K1A 0R6, Canada

Abstract

The NASA Ames real–time wind tunnel wall interference correction system was applied to four geometrically similar flat plates that were tested in the NRC/IAR pilot wind tunnel. The flat plates were tested at on– and off–centerline positions, at angles of attack from $-5°$ to $+110°$. The correction system used wall pressure and lift force measurements in combination with a singularity representation of the flat plates to estimate wall interference corrections. Blockage and angle of attack corrections were computed and applied to lift, drag, and pitching moment coefficients. Corrected lift and pitching moment coefficients show excellent agreement over the whole angle of attack range for all four flat plates. Corrected drag coefficents show excellent agreement up to approximately $50°$ angle of attack. No drag coefficient correction due to the distortion of the separation wake was applied. Therefore, for angles of attack greater than $50°$, small differences between the corrected drag coefficients remain.

Nomenclature

b = $2\ s$; span of reflected flat plate
C = wind tunnel cross–sectional area
c = chord of flat plate
c_D = corrected drag coefficient
c'_D = uncorrected drag coefficient
c_L = corrected lift coefficient
c'_L = uncorrected lift coefficient
c_M = corrected pitching moment coefficient
c'_M = uncorrected pitching moment coefficient
c_p = pressure coefficient during model test
$\overline{c_p}$ = pressure coefficient during calibration
Δc_p = $c_p\ -\ \overline{c_p}$
D = corrected drag force
D' = uncorrected drag force
ΔD = drag force correction
k = singularity index
L = corrected lift force
L' = uncorrected lift force
ΔL = lift force correction
m = total number of wall pressure ports
N = total number of reference points
n = total number of singularities
S = model reference area
s = semispan of flat plate
Δs = span increment
U_c = flow velocity at a wall pressure port during empty tunnel calibration
U_{ref} = test section reference velocity
U_t = flow velocity at a wall pressure port during wind tunnel test
u_i = perturbation velocity of wall interference flow field for unit sing. strength (x–comp.)
$\overline{u_i}$ = u_i/U_{ref}
u_t = perturbation velocity of wind tunnel flow field for unit singularity strength
$\overline{u_t}$ = u_t/U_{ref}
v_i = perturbation velocity of wall interference flow field for unit sing. strength (y–comp.)
$\overline{v_i}$ = v_i/U_{ref}
w = weighting factor (elliptic lift distribution)
x = streamwise coordinate
y = y–coordinate
z = z–coordinate

α = corrected angle of attack
α' = uncorrected angle of attack

* Senior Aerodynamicist, SVERDRUP Technology, Inc.
** Principal Research Officer, Aerodyn. Lab., NRC Canada.

α_i = angle of attack correction at reference point
$\Delta\alpha$ = averaged angle of attack correction
δ = wall pressure port index
ϵ = blockage factor at reference point
ε = averaged blockage factor
η = number of point doublets (volume blockage)
ν = flow field point index
ξ = total number of point doublets
σ_k = singularity strength
σ_* = ref. singularity strength (solid vol. blk.)
σ_{**} = ref. singularity strength (wake blockage)

$\mathbf{A}$ = linear system matrix
$\mathbf{B}$ = right hand side vector
$\mathbf{X}$ = linear system solution vector

Introduction

TWICS, the NASA Ames wind tunnel wall interference correction system, was originally developed for the NASA Ames 11ft Transonic Wind Tunnel (TWT) in order to predict wall interference corrections at high subsonic Mach numbers.[1] During the year 2001 major modifications of the TWICS software were completed. Now it is also possible to apply TWICS to the closed–wall test section of the NASA Ames 12ft Pressure Wind Tunnel (PWT).

TWICS uses a highly modified version of the wall signature method to predict wall interference corrections.[1] Wall pressure, lift force, and pitching moment measurements are combined with solutions of the subsonic potential equation and a singularity representation of the test article in order to determine blockage and angle of attack corrections. Required solutions of the subsonic potential equation for the slotted wall boundary condition (11ft TWT) and the closed wall boundary condition (12ft PWT) are provided by the panel method ANTARES.[2] This panel method code was developed to solve the flow field of a point or line doublet that is placed inside a wind tunnel test section.

In the past, wall interference corrections computed by the TWICS algorithm were successfully validated using classical wall interference flow field solutions that are available for the closed–wall boundary condition. A limited number of known numerical wall interference correction estimates were also used to validate TWICS corrections that are computed for the slotted wall test section of the 11ft TWT. However, due to a lack of suitable test data, no validation of wall interference corrections over a large angle of attack range could be performed.

In January 2002, thanks to the generosity of the Institute for Aerospace Research (IAR) in Ottawa, Canada, data from a wind tunnel test of four flat plates was made available to NASA Ames Research Center. The data offered the opportunity to validate TWICS corrections at high angles of attack with fully separated flows. Four geometrically similar flat plates were tested in the IAR pilot tunnel. One of the objectives of these tests was the evaluation of a two–variable wall interference correction method that is currently being developed at the IAR for correcting low–speed wind tunnel data.[3,4]

After a review of a detailed description of the test set–up (for more detail see Ref. [3]) it was recognized that only minor modifications of the existing TWICS software had to be made in order to process the IAR flat plate data. These changes included (a) the description of the IAR test section geometry, (b) the description of the location of the 240 wall pressure ports of the IAR tunnel, (c) the implementation of the closed wall boundary condition, (d) the description of the rotation and lateral movement of the flat plates, and (e) the conversion of all units to the metric system. In addition, the singularity and reference point input files of the four tested flat plates had to be prepared. All required software modifications were successfully completed within 2 weeks. Afterwards, a detailed analysis of the wall interference corrections of the test data was performed that is reported in this paper.

In the first part of this paper, the test of four flat plates in the IAR pilot wind tunnel is reviewed. Then, the application of the TWICS algorithm to the flat plate test data is discussed in detail. Finally, uncorrected and corrected aerodynamic coefficients are compared and analyzed.

Flat Plate Tests

Lift, drag and pitching moment were measured for a set of four flat–plate, reflection–plane wings in the IAR pilot wind tunnel. Surface pressures were measured simultaneously at 240 locations over 15 longitudinal rows of taps set into the tunnel side walls and ceiling. The pressure data were used for an evaluation of the IAR version of the two–variable method[3,4] and to evaluate an improved pressure–signature method[5]. Force and moment data were used to evaluate a re–derivation of Maskells method for separated flows.[5]

A flat plate geometry was selected because it could be easily replicated in four sizes, could be simply modeled for computational purposes and because it contained the flow physics typical of streamlined and bluff bodies. The leading and trailing edges of the flat plates were beveled on the suction sides to ensure a clean separation that was intended to reduce Reynolds number dependence. The models could be pitched through more than 90°, providing attached and fully

separated flow conditions. This large range was required because the IAR wind tunnels are involved in aeronautical studies at low and high angles of attack as well as in the separated–flow aerodynamics of large civil–engineering structures and surface vehicles.

The measurements were conducted in a closed–return, solid–walled tunnel, having a 914 mm wide by 914 mm high by 2500 mm long test section, a maximum speed of 55 m/s, a turbulence intensity of 0.5 %, and a mean–flow uniformity of ± 0.5 %. The walls diverge and the longitudinal pressure gradient is essentially zero. This wind tunnel is a 10 % scale model of the NRC 9 $m \times 9$ m Low–Speed wind tunnel.

The models were mounted, one at a time, on a six–component balance and turntable assembly situated below the test section floor. Each flat plate has a reflected aspect ratio of 3.0 and a thickness–to–chord ratio of 0.032. A sketch of the experimental setup is shown in Fig. 1. The models were located at $x = 788$ mm downstream of the test section entrance. A special feature of this experimental program was the ability to move the models laterally from the tunnel vertical plane of symmetry. The installation is shown in Fig. 2, where the sliding sealing plate, the edge bevels and the flush pressure rails can be seen. The model was connected to a six-components platform balance on a sliding track. The dimensions of the four models are summarized in Table 1.

Table 1: Flat Plate Model Dimensions

Model	*S/C*	*c* [*m*]	*s* [*m*]
1	0.040	0.149	0.224
2	0.071	0.199	0.299
3	0.111	0.249	0.373
4	0.160	0.299	0.448

The models had scaled mounting bars and scaled root seals to minimize inter–model differences. A preliminary study showed that the model design was Reynolds number insensitive, so all the tests were run at 30 m/s to ensure adequate and uniform pressure measurement accuracy.

TWICS

General Remarks

TWICS uses a modified version of the wall signature method to compute wind tunnel wall interference effects of a test article.[1] A singularity representation of the test article is combined with the measurement of wall pressures, lift force, and precalculated normalized perturbation velocities of the wind tunnel and wall interference flow field to compute corrections.

In this section, the application of TWICS to the IAR flat plate model tests will be discussed. The flat plates are considered to be semispan models assuming that the uncorrected lift force is pointing in the positive y–coordinate direction. The test section floor is the reflection plane. Point doublet chains are used to model blockage effects of a test article.[6] Solid volume and viscous separation wake blockage effects are distinguished. Line doublets are used to represent lifting effects. Table 2 lists singularities that are used by TWICS to represent a test article.

Table 2: Singularity Representation

Phenomenon	*Type*	*Indices*
Solid Vol. Blk.	Point Doublet	$1, \cdots, \eta$
Wake Blockage	Point Doublet	$\eta + 1, \cdots, \xi$
Lifting Effects	Line Doublet	$\xi + 1, \cdots, n$

The initial location of all singularities is specified by the user of TWICS using drawings of the test article. In the case of the flat plates, solid volume blockage was represented by placing a chain of point doublets of equal strength on the floor of the test section. Separation wake blockage effects were represented by placing four chains of point doublets along the semispan of each flat plate. These chains start at the mid–chord of the plate and extend approximately two tunnel widths downstream of the flat plate. Finally, seven equally spaced line doublets were placed along the mid–chord line of each flat plate to model lifting effects.

The blockage factor ϵ and the angle of attack correction α_i are linear functions of the singularity representation of the test article. The principle of superposition may be applied to the wall interference flow field. Therefore, it is possible to express ϵ and α_i at a test article reference point "ν" as the sum of contributions of all test article singularities. Then, assuming that a total number of "n" singularities are used to represent a flat plate, we get:

$$\epsilon(\nu) = \sum_{k=1}^{n} \sigma_k \cdot \overline{u_i}(\nu, k) \qquad (1a)$$

$$\alpha_i(\nu) = \sum_{k=1}^{n} \sigma_k \cdot \overline{v_i}(\nu, k) \qquad (1b)$$

where $\overline{u_i}(\nu, k)$ and $\overline{v_i}(\nu, k)$ are perturbation velocities of the wall interference flow field that are divided by the singularity strength and the reference velocity.

The velocity $\overline{u_i}(\nu,k)$ may be interpreted as the dimensionless axial perturbation velocity of the interference flow field that is caused by a unit strength singularity "k"at a flow field point "ν." The velocity component $\overline{v_i}(\nu,k)$ is the corresponding dimensionless perturbation velocity that is perpendicular to the projected wing plane of the test article.

Perturbation velocities $\overline{u_i}(\nu,k)$ and $\overline{v_i}(\nu,k)$ are computed for a point doublet and a line doublet at a large number of possible singularity locations using the panel method code ANTARES.[2] These perturbation velocities of the wall interference flow field are stored in a database file. TWICS uses this file to perform a real–time interpolation of the perturbation velocities as a function of the singularity type and location.

The strengths of singularities representing each flat plate are determined using (i) the measurement of the lift force and (ii) a least squares fit of the wall pressure signature. The calculation of the singularity strength is explained in the following three sections.

Solid Volume and Wake Blockage Effects

Solid volume blockage effects of a flat plate are represented by a chain of point doublets (singularity indices $1,\cdots,\eta$) that are placed on the test section floor along the chord of the flat plate. The unknown singularity strengths $\sigma_1,\cdots,\sigma_\eta$ of these point doublets are reduced to a single variable σ_* by introducing relative weighting factors. Experience has shown that these weighting factors may be set to one in the case of the flat plate. Then, we obtain:

$$\frac{\sigma_k}{\sigma_*} \quad = \quad 1 \quad ; \quad 1 \le k \le \eta \qquad (2)$$

Separation wake blockage effects are represented by another set of point doublets (singularity indices $\eta+1,\cdots,\xi$). Again, weighting factors are introduced to reduce the number of independent variables during the calculation of the singularity strengths. It is possible to assign a weighting factor of one to all these point doublets. Then, assuming that the strength σ_{**} is a common reference strength of the point doublets representing the separation wake, we get:

$$\frac{\sigma_k}{\sigma_{**}} \quad = \quad 1 \quad ; \quad \eta+1 \le k \le \xi \qquad (3)$$

It will be shown below that the calculation of the strength of point doublets representing test article blockage effects is reduced to finding the values of σ_* and σ_{**} using a least squares fit of the wall signature.

Lifting Effects

The strengths $\sigma_{\xi+1},\cdots,\sigma_n$ of the line doublets representing lifting effects of a flat plate are estimated by combining the lift force measurement with the *Kutta/Joukowski* formula. Line doublet strengths modeling an elliptic lift distribution along the semispan of the flat plate were used to analyze the IAR flat plate data. Therefore, weighting factors $w(k)$ were introduced that model an elliptic lift distribution along the semispan of a flat plate. Then, we get:

$$\sigma_k \quad = \quad \frac{w(k)\cdot c'_L \cdot c \cdot \Delta s}{2} \quad ; \quad \xi+1 \le k \le n \qquad (4a)$$

$$\Delta s \quad = \quad \frac{s}{(n-\xi)} \qquad (4b)$$

$$\sum_{k=\xi+1}^{n} w(k) \quad = \quad 1 \qquad (4c)$$

where c'_L is the uncorrected lift coefficient, c is the chord, and s is the semispan of the flat plate. More detail about the calculation of the strength of a line doublet is given in Ref. [2], App. 3.

Least Squares Fit of Wall Signature

A least squares fit of the wall signature is performed in order to calculate the reference singularity strength values σ_* and σ_{**} that are related to test article blockage effects. TWICS applies a least squares fit to the wall pressure signature that is expressed as a dimensionless perturbation velocity. Therefore, it is necessary to compute an axial velocity $U_t(\delta)$ from wall pressure measurements that are made during the wind tunnel test. Assuming that the wall pressure coefficient $c_p(\delta)$ was measured, we get the following first order approximation of $U_t(\delta)$:

$$U_t(\delta) \quad \approx \quad U_{ref}\cdot\left[\,1 \,+\, \frac{c_p(\delta)}{-2}\,\right] \qquad (5a)$$

where U_{ref} is the reference velocity that was used to compute $c_p(\delta)$. TWICS corrects the wall pressure signature $U_t(\delta)$ for orifice error, wall divergence, and wall boundary layer growth by subtracting the velocity $U_c(\delta)$ of a corresponding empty tunnel calibration at each wall pressure port location. Assuming that the wall pressure coefficient $\overline{c_p}(\delta)$ was measured during an empty tunnel calibration, we get for $U_c(\delta)$:

$$U_c(\delta) \quad \approx \quad U_{ref}\cdot\left[\,1 \,+\, \frac{\overline{c_p}(\delta)}{-2}\,\right] \qquad (5b)$$

Wall pressure signatures used in the present study were supplied as pressure coefficient differences $\Delta c_p(\delta)$. These differences are defined as:

$$\Delta c_p(\delta) \quad = \quad c_p(\delta) \,-\, \overline{c_p}(\delta) \qquad (5c)$$

Then, combining Eqs. (5a), (5b), and (5c) and after some algebra, we get the following first order approximation of the wall pressure signature difference:

$$\frac{U_t(\delta) \; - \; U_c(\delta)}{U_{ref}} \quad \approx \quad \frac{\Delta c_p(\delta)}{-2} \qquad (5d)$$

It is assumed that measurements at a total number of "m" wall pressure ports are used for the least squares fit of the wall pressure signature. A total number of "n" singularities is selected to represent the test article. Then, the normal equation of the least squares fit of the wall signature may be written as:

$$\left[\mathbf{A^T}_{2\times m} \circ \mathbf{A}_{m\times 2}\right] \circ \mathbf{X}_{2\times 1} \; = \; \mathbf{A^T}_{2\times m} \circ \mathbf{B}_{m\times 1} \qquad (6a)$$

$$\mathbf{X}_{2\times 1} \quad = \quad \begin{pmatrix} \sigma_* \\ \sigma_{**} \end{pmatrix} \qquad (6b)$$

$$\mathbf{A}_{m\times 2} \quad = \quad \begin{pmatrix} a_{1,1} & a_{1,2} \\ \vdots & \vdots \\ a_{m,1} & a_{m,2} \end{pmatrix} \qquad (6c)$$

$$a_{\delta,1} \quad = \quad \sum_{k=1}^{\eta} \overline{u_t}(\delta,k) \qquad (6d)$$

$$a_{\delta,2} \quad = \quad \sum_{k=\eta+1}^{\xi} \overline{u_t}(\delta,k) \qquad (6e)$$

$$\mathbf{B}_{m\times 1} \quad = \quad \begin{pmatrix} b_1 \\ \vdots \\ b_m \end{pmatrix} \qquad (6f)$$

$$b_\delta \quad = \quad \frac{\Delta c_p(\delta)}{-2} \; - \; \sum_{k=\xi+1}^{n} \sigma_k \cdot \overline{u_t}(\delta,k) \qquad (6g)$$

The vector $\mathbf{X}$ contains the strength of singularities modeling test article blockage effects. Matrix $\mathbf{A}$ contains dimensionless perturbation velocities of the wind tunnel flow field. The vector $\mathbf{B}$ contains perturbation velocities caused by test article blockage effects. Components of vector $\mathbf{B}$ are computed by subtracting line doublet contributions (indices $\xi+1, \cdots, n$) from the measured wall signature difference.

Perturbation velocity $\overline{u_t}(\delta,k)$ is the dimensionless perturbation velocity of the wind tunnel flow field that is caused by a singularity "k" at a wall pressure port "δ." It is the perturbation velocity of the wind tunnel flow field at the wall pressure port divided by the singularity strength and the reference velocity. Similar to $\overline{u_i}(\nu,k)$ and $\overline{v_i}(\nu,k)$, the panel method code ANTARES may be used to compute $\overline{u_t}(\delta,k)$ as a function of the singularity type and possible singularity locations. Perturbation velocities are again stored in a database file that is used by TWICS for interpolation purposes. Table 3 lists differences between $\overline{u_i}(\nu,k)$, $\overline{v_i}(\nu,k)$, and $\overline{u_t}(\delta,k)$.

Table 3: Perturbation Velocity Differences

Velocity	*Flow Field Type*	*Point Type*
$\overline{u_i}(\nu,k)$ $\overline{v_i}(\nu,k)$	Wall Interference Flow Field	Reference Point
$\overline{u_t}(\delta,k)$	Wind Tunnel Flow Field	Wall Pressure Port

The solution of the least squares problem defined in Eq. (6a) can be written in explicit form as:

$$\mathbf{X}_{2\times 1} \; = \; \left[\mathbf{A^T} \circ \mathbf{A}\right]^{-1}_{2\times 2} \quad \circ \quad \left[\mathbf{A^T} \circ \mathbf{B}\right]_{2\times 1} \qquad (7)$$

The solution vector $\mathbf{X}$ is computed by using a linear system solver. Then, type, location, and strength (i.e. $\sigma_1, \cdots, \sigma_n$) of all singularities representing the flat plate are known. It is now possible to determine the blockage factor ϵ and the angle of attack correction α_i at a reference point "ν" using Eqs. (1a) and (1b).

Application of Corrections

After the solution of the least squares fit of the wall signature is found, the blockage factor $\epsilon(\nu)$ and the angle of attack correction $\alpha_i(\nu)$ at each model reference point ν can be determined. Following a suggestion made in Ref. [3], $\epsilon(\nu)$ and $\alpha_i(\nu)$ are computed at reference points that are located along the mid–chord of the flat plate. Then, weighted averages ε and $\Delta\alpha$ of the blockage factor and of the angle of attack correction are determined. We get:

$$\varepsilon \quad = \quad \sum_{\nu=1}^{N} w(\nu) \cdot \epsilon(\nu) \qquad (8a)$$

$$\Delta\alpha \quad = \quad \sum_{\nu=1}^{N} w(\nu) \cdot \alpha_i(\nu) \qquad (8b)$$

where $w(1), \cdots, w(N)$ are weighting factors that represent an elliptic lift distribution along the mid–chord of the flat plate. They fulfill the condition:

$$\sum_{\nu=1}^{N} w(\nu) \quad = \quad 1 \qquad (8c)$$

The averaged blockage factor and angle of attack correction are combined with the TWICS correction equations to determine corrected aerodynamic coefficients and the corrected angle of attack of the flat plate. This is done in six steps:

Step 1: The uncorrected lift and drag force are determined using the uncorrected lift and drag coefficients, the uncorrected dynamic pressure, and the model reference area. Then, we get:

$$L' = c'_L \cdot S \cdot q' \quad (9a)$$

$$D' = c'_D \cdot S \cdot q' \quad (9b)$$

Step 2: Lift and drag force corrections caused by the wall interference induced inclination of the lift and drag force vectors are computed using the formulæ:[7]

$$\Delta L = -D' \cdot sin\ \Delta\alpha + L' \cdot [\ cos\ \Delta\alpha - 1\ ] \quad (10a)$$

$$\Delta D = D' \cdot [\ cos\ \Delta\alpha - 1\ ] + L' \cdot sin\ \Delta\alpha \quad (10b)$$

Step 3: Corrected lift and drag forces are computed by adding corrections to the uncorrected forces:

$$L = L' + \Delta L \quad (11a)$$

$$D = D' + \Delta D \quad (11b)$$

Step 4: The corrected dynamic pressure is determined using the uncorrected dynamic pressure and the averaged blockage factor:

$$q = q' \cdot \left[\ 1 + 2 \cdot \varepsilon + \varepsilon^2\ \right] \quad (12)$$

Step 5: Corrected aerodynamic coefficients are computed by using corrected forces, the corrected dynamic pressure, and the reference area:

$$c_L = \frac{L}{q \cdot S} \quad (13a)$$

$$c_D = \frac{D}{q \cdot S} \quad (13b)$$

$$c_M = c'_M \cdot \frac{q'}{q} \quad (13c)$$

Step 6: The corrected angle of attack is determined by adding the averaged angle of attack correction to the uncorrected angle of attack:

$$\alpha = \alpha' + \Delta\alpha \quad (14)$$

No stream curvature corrections were applied to the coefficients. In the next section of this paper, uncorrected and corrected aerodynamic coefficients of the IAR flat plate tests will be compared in detail.

Discussion of Results

Lift, drag, and pitching moment measurements were made during the four flat plate tests. Each of the flat plates was mounted on the tunnel centerline and pitched from $-5°$ to $+110°$. Then, all flat plates were mounted at off–center locations and pitched again through the same angle of attack range.

Force data were successfully recorded for all four flat plates. Figure 3a shows the corresponding uncorrected lift coefficient as a function of the uncorrected angle of attack. Figure 4a shows the uncorrected drag coefficient as a function of the uncorrected angle of attack. Moment data were measured successfully only for Model 3 and Model 4. Figure 5a shows the corresponding uncorrected pitching moment coefficient as a function of the uncorrected angle of attack.

Wall interference corrections were computed and applied to the aerodynamic coefficients and the angle of attack as outlined in the previous sections. Figures 3b, 4b, and 5b show the corrected lift, drag, and pitching moment coefficients as a function of the corrected angle of attack. In general, corrected lift and pitching moment coefficients for on– and off–center locations of the model show excellent agreement over the entire angle of attack range.

Comparing Fig. 4a with Fig. 4b we see that the corrected drag coefficients show good agreement up to an angle of attack of $\approx 50°$. Noticable differences between the corrected drag coefficients exist for angles of attack greater than $50°$. These differences are caused by the fact that no correction for wall–interference–induced wake distortion is applied to the uncorrected drag force (see Eq. (11*b*)). TWICS was designed to estimate wall interference effects for the entire subsonic Mach number range. A wake distortion correction procedure similar to the *Maskell III* technique[5] is not yet available for this Mach number range and was therefore not included in the TWICS correction equations.

A simple statistical analysis was performed in order to quantify differences between uncorrected and corrected aerodynamic coefficients. At first, all coefficients were approximated over the entire angle of attack range by piecewise linear functions. Two angle of attack ranges were selected for the analysis, i.e. a low angle of attack range ($-5° \le \alpha, \alpha' \le +20°$) and a high angle of attack range ($+20° \le \alpha, \alpha' \le +110°$). Then, each angle of attack range was divided into a large number of discrete angles. In the next step, the standard deviation of the coefficient at each discrete angle was computed by using the arithmetic mean of the coefficient as an approximation of the interference free "true" value. Finally, the arithmetic mean of the standard deviation over the selected angle of attack range was computed for each uncorrected and corrected coefficient. Table 4 shows the result of this calculation for the two selected angle of attack ranges.

Comparing the standard deviation of the uncorrected lift coefficients with the standard deviation of the corrected lift coefficients we see that the standard deviation of the corrected lift coefficients is more or less independent of the angle of attack. The reductions of the standard deviation of the corrected drag and pitching moment coefficients, however, appear to be larger in the high angle of attack range.

Table 4: Standard Deviation Comparison

Standard Deviation (*uncorrected data*)	*Standard Deviation* (*corrected data*)
$-5^\circ \leq \alpha' \leq +20^\circ$	$-5^\circ \leq \alpha \leq +20^\circ$
$c'_L(\alpha') \Longrightarrow 0.0290$	$c_L(\alpha) \Longrightarrow 0.0100$
$c'_D(\alpha') \Longrightarrow 0.0095$	$c_D(\alpha) \Longrightarrow 0.0061$
$c'_M(\alpha') \Longrightarrow 0.0028$	$c_M(\alpha) \Longrightarrow 0.0027$
$+20^\circ \leq \alpha' \leq +110^\circ$	$+20^\circ \leq \alpha \leq +110^\circ$
$c'_L(\alpha') \Longrightarrow 0.0606$	$c_L(\alpha) \Longrightarrow 0.0111$
$c'_D(\alpha') \Longrightarrow 0.1849$	$c_D(\alpha) \Longrightarrow 0.0347$
$c'_M(\alpha') \Longrightarrow 0.0064$	$c_M(\alpha) \Longrightarrow 0.0020$

A detailed analysis of the force and moment measurements in the IAR tunnel showed that estimated systematic errors of the force measurements were much smaller than systematic errors of the moment measurement. This could explain the fact that the standard deviation reduction of the force coefficients is, in general, much greater than the standard deviation reduction of the moment coefficients.

Conclusion

TWICS, the real–time wall interference correction system of NASA Ames wind tunnels, was applied to a family of four, different sized flat plate models that were tested in the NRC/IAR pilot wind tunnel. Corrected lift and pitching moment coefficients show excellent agreement over the entire angle of attack range. Corrected drag coefficients show excellent agreement up to approximately 50° angle of attack. No drag coefficient correction due to the distortion of the separation wake was applied. Therefore, for angles of attack greater than 50°, small differences between the corrected drag coefficients remain.

In the past, wall interference corrections computed by the TWICS algorithm were successfully compared with corrections that were obtained using the two–variable method or classical techniques. This "indirect" validation of the corrections is acceptable. However, the successful application of the TWICS algorithm to the series of NRC flat plate model tests is the first time that a "direct" validation of the corrections up to large angles of attack has been performed.

Wall interference correction methods always use simplifying assumptions to describe the wall interference flow field. Each method also has to deal with different types of numerical errors. A simple statistical analysis of the aerodynamic coefficients is presented in this paper that may be used to evalute and compare different wall interference correction methods.

Wind tunnel experiments will continue to play a critical role in design and testing of airplanes that are operated at high angles of attack ($\gg 20^\circ$). Reliable wall interference correction methods are needed in that part of the flight envelope. Flat plate models are simple and not expensive to manufacture. Therefore, they represent an affordable way to perform a "direct" validation of these types of correction methods.

Acknowledgment

The authors like to thank Alan Boone of NASA Ames Research Center and Dr. S. Zan and Dr. M. Mokry of the Institute for Aerospace Research, NRC Canada, for their constructive review of the manuscript.

References

[1]Ulbrich, N. and Boone, A. R., "Determination of the Boundary Condition of the NASA Ames 11ft Transonic Wind Tunnel," AIAA 2001–1112, presented at the 39th Aerospace Sciences Meeting, Reno, Nevada, January 8–11, 2001.

[2]Ulbrich, N., "Description of Panel Method Code ANTARES," NASA/CR–2000–209592, contractor report, NASA Ames Research Center, Moffett Field, California, May 2000.

[3]Cooper, K. R. and Mokry, M., "Further Development of the IAR Two–Variable Method for Correcting Low–Speed Wind Tunnel Data," AIAA 2002–0884, presented at the 40th Aerospace Sciences Meeting, Reno, Nevada, January 14–17, 2002.

[4]Mokry, M., "Automation of Wall Interference Procedures Using the C++ Object–Oriented Approach," AIAA 2000–0674, presented at the 38th Aerospace Sciences Meeting, Reno, Nevada, January 10–13, 2000.

[5]Hackett, J. E. and Cooper, K. R., "Extensions to Maskell's Theory for Blockage Effects on Bluff Bodies in a Closed Wind Tunnel," *The Aeronautical Journal of the Roy. Aero. Soc.*, August 2001, pp. 409–418.

[6]Ulbrich, N., "The Representation of Wind Tunnel Model Blockage Effects Using Point Doublets,"

AIAA 2002–0880, presented at the 40th Aerospace Sciences Meeting, Reno, Nevada, January 14–17, 2002.

[7]Ulbrich, N., "The Real–Time Wall Interference Correction System of the NASA Ames 12–Foot Pressure Wind Tunnel," NASA/CR–1998–208537, NASA Ames Research Center, Moffett Field, California, July 1998, App.17.

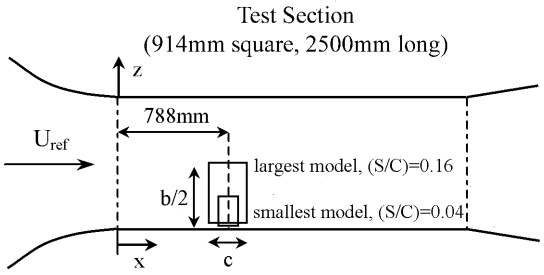

Fig. 1 Tunnel and model dimensions.

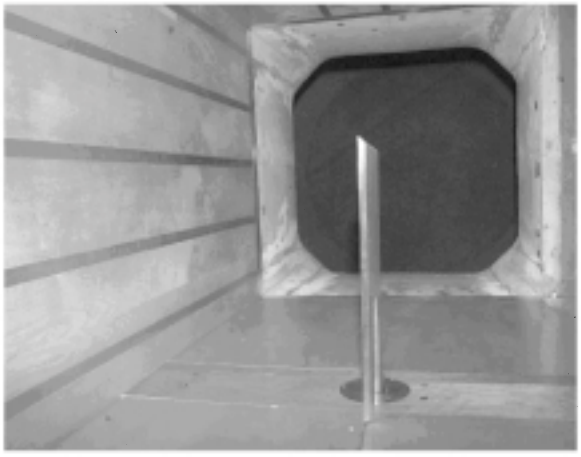

Fig. 2 Model 3 installed in the IAR pilot tunnel at $\alpha = 0°$.

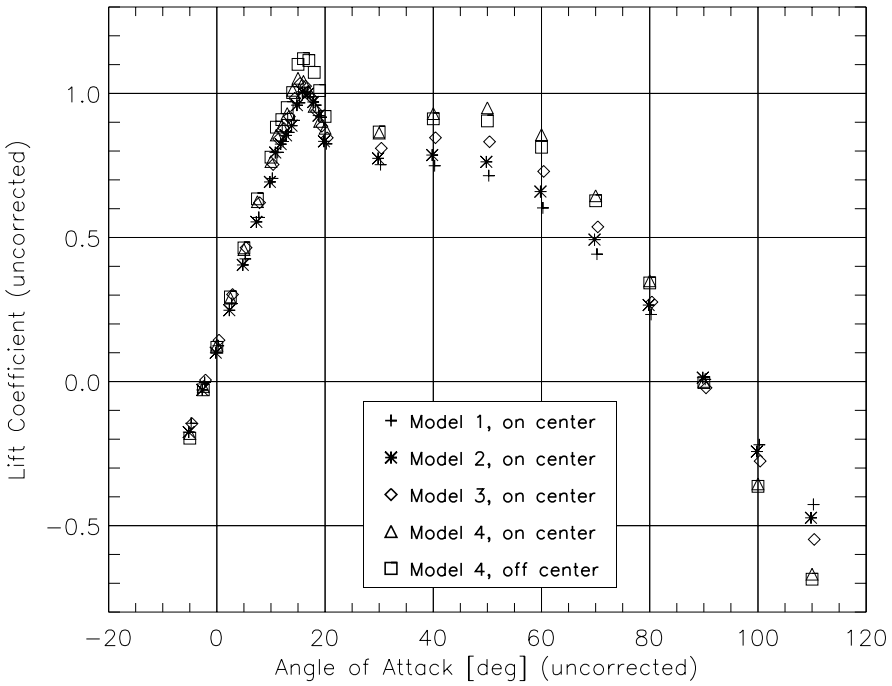

Fig. 3a Uncorrected lift coefficient of flat plate test.

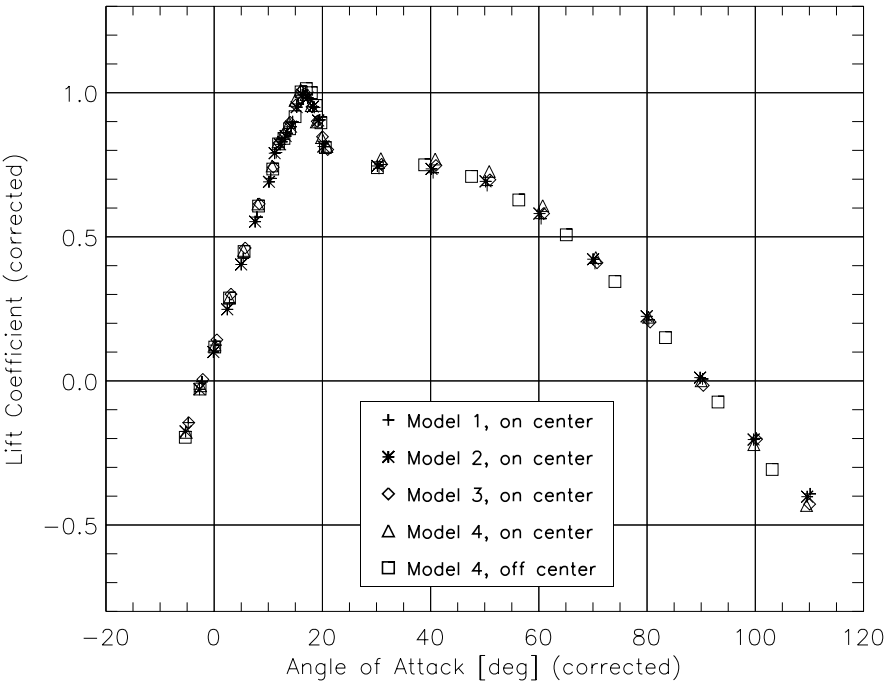

Fig. 3b Corrected lift coefficient of flat plate test.

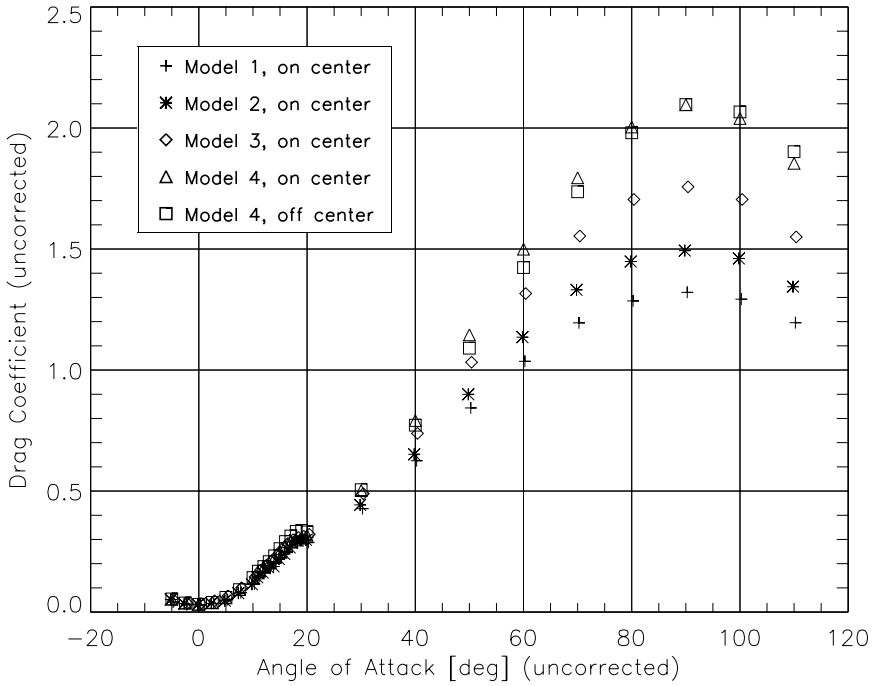

Fig. 4a Uncorrected drag coefficient of flat plate test.

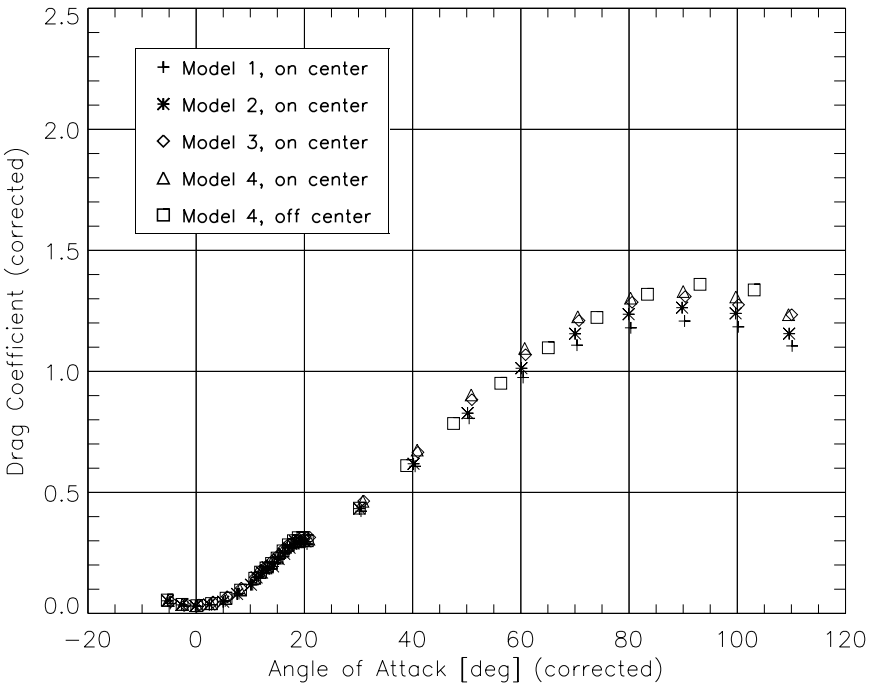

Fig. 4b Corrected drag coefficient of flat plate test.

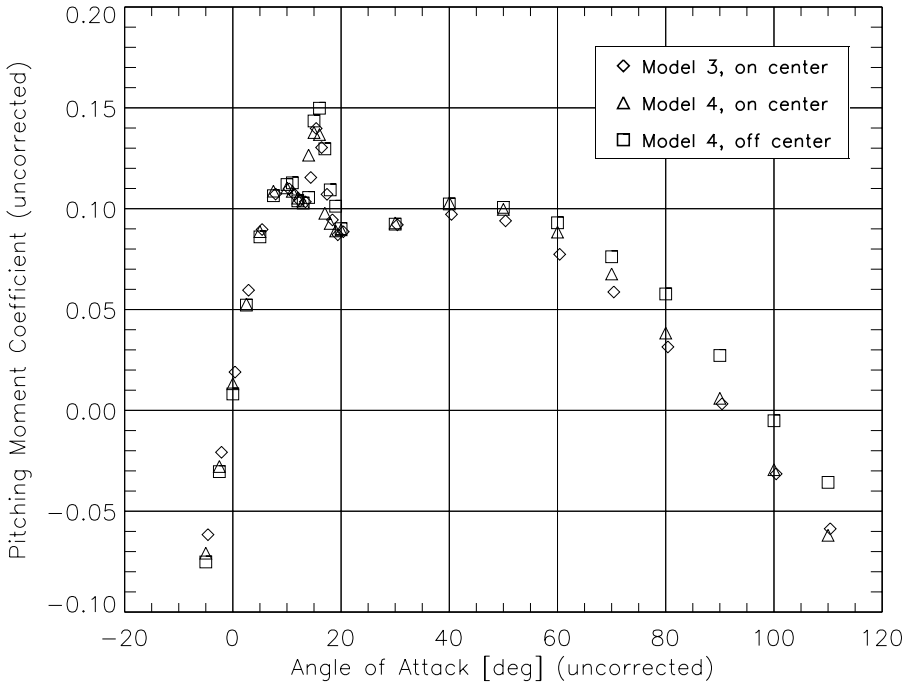

Fig. 5a Uncorrected pitching moment coefficient of flat plate test.

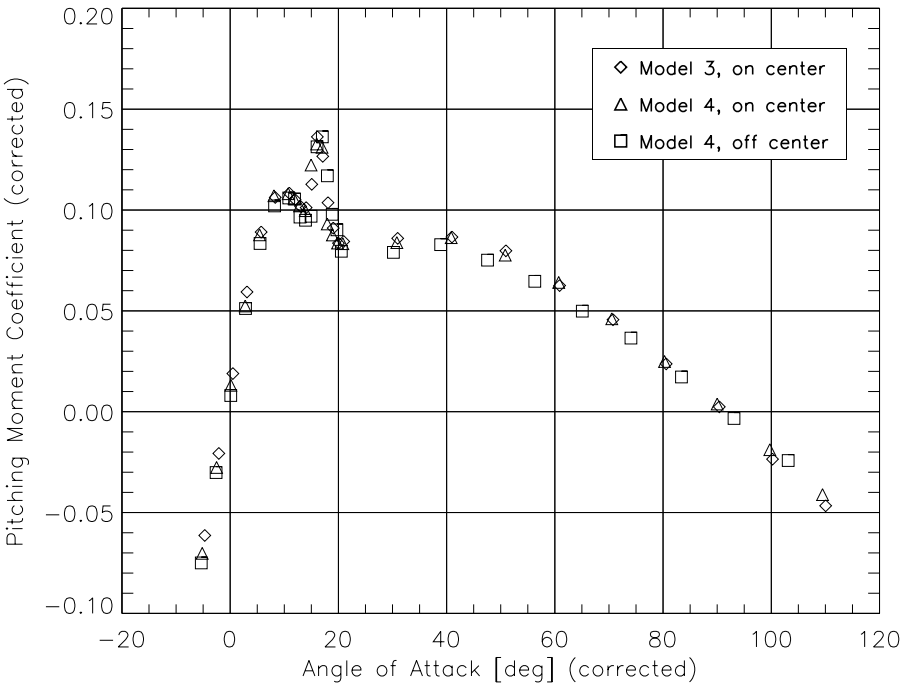

Fig. 5b Corrected pitching moment coefficient of flat plate test.